ELSEVIER

Mechanics of Materials 25 (1997) 291–308

MECHANICS OF MATERIALS

Limitations on the use of the mixed-mode delaminating beam test specimen: Effects of the size of the region of K-dominance

T.L. Becker Jr. [b], J.M. McNaney [a], R.M. Cannon [a], R.O. Ritchie [a,*]

[a] *Materials Sciences Division, Lawrence Berkeley National Laboratory, and Department of Materials Science and Mineral Engineering, University of California, Berkeley, CA 94720-1760, USA*

[b] *Department of Mechanical Engineering, University of California, Berkeley, CA 94720-1760, USA*

Received 25 July 1996; received in revised form 25 February 1997; accepted 28 February 1997

Abstract

The mixed-mode delaminating beam (MMDB) is a widely used test geometry designed to measure the fracture resistance of bimaterial interfaces under mixed-mode loading conditions. In the present work, linear-elastic finite element analyses are employed to determine the complex stress intensity factor, K, for an interfacial crack in this sample; results are found to confirm those of previous studies of the bilayer specimen. However, the numerical results further reveal that the region of K-dominance near the crack tip is very limited, extending merely $\sim 1/100$ to $1/1000$ of the sample height, about an order of magnitude smaller than for other common fracture-mechanics test samples. Analyses performed for this specimen geometry modified to include a thin sandwiched interlayer also indicate a very limited region of K-dominance, for example, extending $\sim 1/10$ of the height of the sandwiched layer from the crack tip for very thin sandwiched layers. For the sandwiched geometry, two situations leading to a useful small scale yielding condition are described. Examples of the use of this specimen in the evaluation of the fracture toughness of ceramic joints are cited from the literature and comparisons are made between the size of the K-dominant region and the extent of crack tip plasticity. Based on these comparisons, the geometry-independent predictive power of linear-elastic fracture mechanics for common bimaterial couples and specimen dimensions using this geometry is challenged.

Keywords: Interface fracture; K-dominance; Small scale yielding; MMDB specimen

1. Introduction

The fracture of materials at, or near, internal interfaces is a failure event critical to the strength and toughness behavior of composites (e.g., debonding of fiber reinforcements), the structural integrity of thin films (e.g., film decohesion) and in microelectronics packaging (Evans et al., 1987; Drory et al., 1988). Invariably, such failures are mixed-mode in nature, with the crack loaded in both tension and shear; the relative magnitude of these modes is characterized by a phase angle, Ψ.

As the fracture resistance of bimaterial interfaces is a strong function of this mode mixity, several specimen geometries have been developed to measure interfacial fracture toughness under mixed-mode

* Corresponding author. Tel.: +1-510-4865946; fax: +1-510-4864995; e-mail: tjbecker@uclink4.berkeley.edu.

PII S0167-6636(97)00010-0

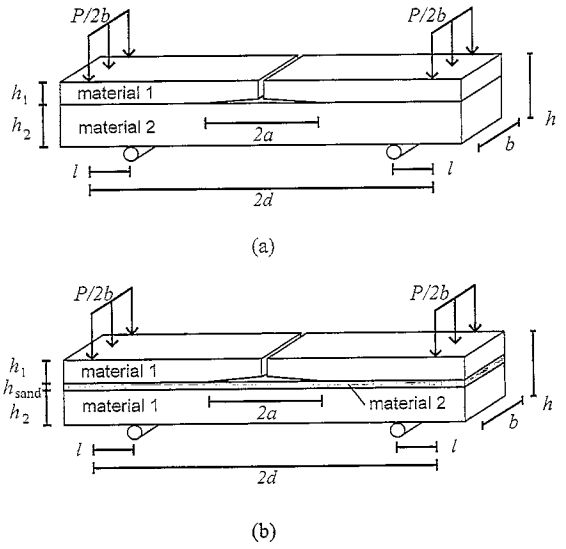

Fig. 1. Mixed-mode delaminating beam test specimen (MMDB), showing (a) the bilayer specimen, with unit height, h, $l = 2h$, $2a = 3h$, $2d = 10h$, and $b = h$ and (b) the modified specimen containing a *sandwiched* interlayer with height h_{sand}. The crack is grown between the top layer and the sandwiched layer.

conditions (O'Dowd et al., 1992). One popular specimen geometry is the mixed-mode delaminating beam (MMDB) test specimen (sometimes referred to as the 'UCSB' specimen). In this geometry (Fig. 1a), the degree of mode mixity can be varied by changing the relative heights (h_1, h_2) of the bimaterial layers, such that crack-growth characteristics for a given material couple can be determined over a range of phase angles (Charalambides et al., 1989). This geometry can also be used with a thin sandwiched interlayer (usually a metal foil) (Fig. 1b). The sandwiched layer is constrained by the top layer and the substrate, which reduces or eliminates the driving force for crack extension due to residual stresses and limits the extent of plastic deformation in the sample.

Since both these specimen configurations have been used to test a large range of material pairs, the purpose of the current work is to re-examine the validity of this specimen geometry for linear-elastic fracture mechanics based studies, specifically by investigating the extent of the region of dominance of the stress singularity (the K-dominance) near the crack tip.

2. Background

2.1. Mechanics of interface cracks

2.1.1. Linear-elastic fracture mechanics (LEFM) solutions

The characteristics of the local stress and displacement fields for a crack lying at the interface between two elastic materials are different from that of a crack in monolithic solid due to the discontinuity in elastic properties across the interface. This elastic mismatch can be characterized by two non-dimensional groups (Dundurs, 1969) known as the Dundurs' parameters α and β:

$$\alpha = \frac{E_1' - E_2'}{E_1' + E_2'} \text{ and}$$

$$\beta = \frac{1}{2}\frac{\mu_1(1-2\nu_2) - \mu_2(1-2\nu_1)}{\mu_1(1-\nu_2) + \mu_2(1-\nu_1)}, \tag{1}$$

where for materials $i = 1$ lying above the crack and 2 below, μ_i are the elastic shear moduli, ν_i are the Poisson's ratios and E_i' are the Young's moduli, E_i, in plane stress or $E_i/(1-\nu_i^2)$ in plane strain. Note that α and β are zero when the materials 1 and 2 have identical elastic properties. For in-plane loading, the stress field at a radial distance r from the tip of a linear-elastic interfacial crack can be expressed as a series of the form (Rice, 1988; Rice et al., 1990):

$$\sigma_{jk} = \frac{1}{\sqrt{2\pi r}}\left[\mathrm{Re}(\boldsymbol{K}r^{i\varepsilon})\Sigma_{jk}^{I}(\varepsilon,\theta) + \mathrm{Im}(\boldsymbol{K}r^{i\varepsilon})\Sigma_{jk}^{II}(\varepsilon,\theta)\right] + Tf_{jk}(\theta) + o(r^{1/2+i\varepsilon}), \quad j,k = r,\theta, \tag{2}$$

where $i = \sqrt{-1}$, $\boldsymbol{K}$ is the complex interface stress intensity ($\boldsymbol{K} = K_1 + iK_2$), θ is the angle from the crack plane and ε is the oscillation index, defined as:

$$\varepsilon = \frac{1}{2\pi}\ln\left(\frac{1-\beta}{1+\beta}\right). \tag{3}$$

Expressions for $\Sigma_{jk}(\varepsilon,\theta)$ are given in Appendix A. The second term in Eq. (2) converts to a xx-stress which is spatially constant except for being discontinuous across the interface (the 'T-stress'). The

corresponding strain-energy release rate G can be calculated for plane-strain conditions as (Rice et al., 1990):

$$G = \frac{[(1-\nu_1)/\mu_1 + (1-\nu_2)/\mu_2]|K|^2}{4\cosh^2(\pi\varepsilon)}, \qquad (4)$$

where $1/\cosh^2(\pi\varepsilon)$ is equal to $(1-\beta^2)$.

2.1.2. Region of K-dominance

It is clear that as $r \to 0$, the magnitudes of the higher order terms in Eq. (2) are negligible when compared to the leading term. In this region, the magnitudes of the singularities in the stress components are scaled by the complex interface stress intensity K and this defines the region of K-dominance in the vicinity of the crack tip. As r increases, the relative magnitudes of the higher order terms increase and the stress field will no longer be well-characterized by K. The requirement that this region envelops the relevant fracture processes is the basis of geometry-independent LEFM-based fracture testing.

The size of the region of K-dominance, extending a distance r_K from the crack tip, is often scaled by the smallest dimension of a finite body (or the crack length in an infinite body) such that with smaller specimen dimensions there is a smaller region of K-dominance. The sign and magnitude of the deviation of the stresses from the K-field is also a function of the shape of the body; indeed, different specimen geometries are known to have varying extents of K-dominance (Fig. 2) (Knott, 1973). For interfacial cracks, this is also a function of the degree of elastic mismatch across the interface (Gu, 1993). The size of the region of K-dominance in a homogeneous body (one with $\alpha = \beta = 0$) is of particular interest in this study and is denoted r_K^H.

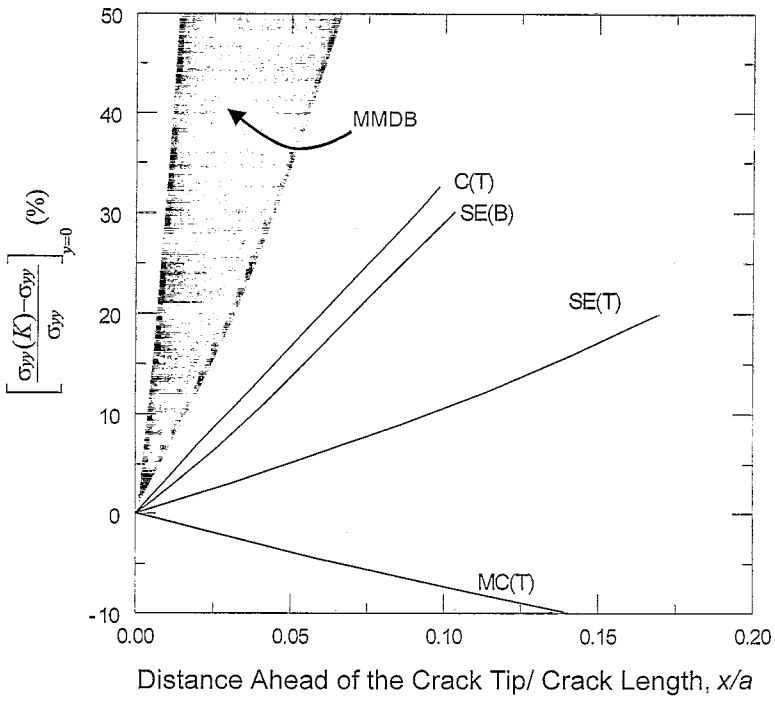

Fig. 2. Deviation of the tensile-opening stress component, σ_{yy}, from the K-field with normalized distance, x/a, directly ahead of a crack, of length a, in a number of common fracture mechanics test samples. It is apparent that the K-field shows a considerable tendency to over-predict the yy-stresses in the homogeneous mixed-mode delaminating beam (MMDB) geometry when compared to the compact-tension (C(T)), single-edge notch bend bar (SE(B)), single-edge notch tensile bar (SE(T)) and middle-cracked tensile sheet (MC(T)). Data for the C(T), SE(B), SE(T) and MC(T) specimens taken from Knott (1973).

2.1.3. Phase angle

The complex interface stress intensities in Eq. (2) only appear in the grouping $Kr^{i\varepsilon}$ with units of (stress)(length)$^{1/2}$ (e.g., MPa $\sqrt{m}$). The real and imaginary parts of this group can be used to form an interface phase angle, $\Psi = \tan^{-1}[\mathrm{Im}(Kr^{i\varepsilon})/\mathrm{Re}(Kr^{i\varepsilon})]$, which in turn can be used, as in the case of a crack in a monolithic solid, to describe the ratio of the shear and normal stresses ahead of the crack, $\sigma_{xy}/\sigma_{yy}|_{y=0} = \tan\Psi$. In the monolithic case, the phase angle is constant within the region of K-dominance and is a unique function of the geometry and loading. For the interface crack, however, the phase angle depends as well on the distance along the interface ahead of the crack tip, x, such that the ratio of shear to normal stresses on the interface is a function of x.

To describe the spatial dependence of the mode mixity, a reference phase angle Ψ^* can be used to describe a given geometry and far-field loading through $\Psi^* = \tan^{-1}[\mathrm{Im}(KL^{i\varepsilon})/\mathrm{Re}(KL^{i\varepsilon})]$, where L is an arbitrary reference distance from the crack tip, such as a specimen dimension (e.g., the total beam height, h) or a microstructurally relevant size-scale, such as the grain size. It is important to note that this phase angle is a characteristic of the interface stress intensity, although the reference distance L may be well outside the region of K-dominance. The angle Ψ^* is purely a reference number which can be used to calculate Ψ at any distance ahead of the crack tip via the relationship (Rice et al., 1990):

$$\Psi = \Psi^* + \varepsilon \ln\left(\frac{x}{L}\right). \tag{5}$$

In Eq. (5), ε effectively scales the rate of change of the local phase angle, Ψ, with the logarithm of distance from the crack tip and Eq. (5) is pertinent within the range of K-dominance, even if L (and consequently Ψ^*) is not.

2.1.4. Crack face interpenetration

The linear-elastic solution for the displacement fields in the vicinity of an interface crack predicts that at distances very close to the crack tip (at $r = r_{\mathrm{int}}$), the crack faces will interpenetrate (England, 1965; Comninou, 1990; Rice, 1988); the radius over which this occurs is governed by the Dundurs' parameter β and the reference phase angle Ψ^*, but is independent of the magnitude of the far-field loading. In a physical body the crack faces do not actually interpenetrate, rather a small zone of contact between the crack faces is established. This contact violates the assumption of traction-free crack faces posed in this elastic boundary value problem [1]. The area over which interpenetration is predicted must therefore be much smaller than the region of K-dominance i.e., $r_{\mathrm{int}} \ll r_K$, for LEFM to accurately characterize the state of stress around the crack.

2.1.5. Near-tip plasticity for interfacial cracks

If plastic deformation occurs in either of the materials across the interface, then the yielding that occurs at the crack tip will cause the local stress field to deviate from the singular stress form of Eq. (2). The size of the plastic-zone, r_p, is defined as the maximum radial distance from the tip to the elastic–plastic boundary. The condition of *small scale yielding* (SSY) is achieved providing the extent of local yielding remains small compared to the region of K-dominance i.e., $r_p \ll r_K$. Here, the stresses within the plastic zone are still scaled by the magnitude of the stress intensity factor and characterization of the crack-tip fields in terms of K will still be valid (Rice, 1974).

The problem of a crack between two bonded, elastic–plastic half-spaces was analyzed by Shih (1991). The plastic zone size in this infinite-body, r_p^∞, can be calculated in terms of the yield stress of the weaker material, σ_y, as:

$$r_p^\infty = \Lambda(\xi)\frac{|K|^2}{\sigma_y^2}, \tag{6}$$

where $\Lambda(\xi)$ is a dimensionless function of the plastic phase angle, ξ:

$$\xi = \Psi^* + \varepsilon \ln\left(\frac{|K|^2}{\sigma_y^2 L}\right). \tag{7}$$

The superscript ∞ is used to denote that this analysis pertains when the plastic zone is much smaller than all other specimen dimensions.

[1] However, since a linear finite element formulation is used in the current study (i.e. involving a solution determined in the reference configuration) such interpenetration will have no effect on the numerical computations of the crack-tip fields.

2.2. The bilayer MMDB specimen

Previous analytical and numerical studies on the bilayer mixed-mode delaminating beam (MMDB) specimen (Fig. 1a) have shown that for interfacial cracks within the constant moment region (between the inner two loading points), the strain-energy release rate does not change with crack length. Charalambides et al. (1989) formulated an analysis based on Bernoulli–Euler beam theory in order to compute the strain-energy release rate, G_{ss}, for interface cracks in this 'steady-state' region; Suo and Hutchinson (1990) extended this analysis reporting semi-analytical values for $\boldsymbol{K}$ (from which both G_{ss} and the reference phase angle Ψ^* can be calculated). These studies report trends of markedly decreasing G_{ss} with increasing substrate stiffness, E_2/E_1 (i.e., decreasing α) and of increasing Ψ^* (referenced to the beam height, h) from ~ 45 to 60° with increasing modulus mismatch. Whereas G_{ss} was found to be only a function of α (and specimen geometry), the value of the phase angle is a function of both α and β.

The results of finite element analyses of this specimen (Charalambides et al., 1989) were in agreement with the semi-analytical results of Suo and Hutchinson (1990). In addition, computations of G and Ψ^* were developed for cracks extending beyond the steady-state region and effects of residual thermal stresses and frictional loading were considered (Charalambides et al., 1990).

2.3. The sandwiched MMDB specimen

There has not been a formal analysis of effects of the sandwiched layer on the strain-energy release rate G and reference phase angle Ψ^* of the sandwiched mixed-mode delaminating beam sample (Fig. 1b). A finite element analysis of the MMDB sample with a sandwiched interlayer for a glass/epoxy system revealed shifts in Ψ^* ($\sim 10°$) and slight changes in G ($\sim 1\%$) for thin epoxy layers $\sim h_{sand}/h = 2\%$ (Ritter et al., 1994). Usually the strain-energy release rate for this sample has been approximated by using the calibration for the bilayer sample, assuming the elastic properties of the sandwiched layer are identical to those of the substrate, or that the interlayer is negligibly thin.

The analysis of Suo and Hutchinson (1990) for the MMDB specimen, in combination with their earlier asymptotic analysis (Suo and Hutchinson, 1989) for bodies containing sandwiched layers, may serve as a suitable approximation for sandwiched layers that are very thin compared to the overall height of the sample (i.e., $h_{sand} \ll h$). In this situation, the strain-energy release rate is equal to that of the homogeneous bilayer sample and the phase angle is shifted from that of the homogeneous sample by an amount depending on the compliance mismatch (α, β) and on h_{sand}. However, for such an asymptotic analysis to be applicable, there must be a region outside of the layer which is described by the K-field for the homogeneous material (i.e., $h_{sand} \ll r_K^H$). Moreover, there is also a much smaller region embedded within this where the interface field pertains, which can be described as the interfacial K-dominant region with size r_K. The size of the K-field in a homogeneous MMDB, r_K^H, is used in this study to determine when such asymptotic limits are met.

2.4. Previous methods of finite element / fracture mechanics analysis

Two methods of data reduction were employed in previous finite element studies to calculate the complex interface stress intensity $\boldsymbol{K}$ (or equivalently G and Ψ^*) for the MMDB geometry. The first involved taking values from finite element computations of the crack-face displacements to calculate the real and imaginary parts of $\boldsymbol{K}h^{i\varepsilon}$ (Charalambides et al., 1989) and the second used a virtual crack-extension technique (Matos et al., 1989). The latter method was considered to be superior because of its insensitivity to mesh refinement, i.e., its ability to yield accurate results even with coarse meshes. However, since this method does not focus on the finite element solution in the near-tip region, the issue of K-dominance was not considered. In discussion of their results, Charalambides et al. (1989) did note that there was some disagreement between the results of the two methods; however, the authors attributed this entirely to errors in the finite element analysis at the crack tip.

It is a contention motivating the present study that the virtual crack-extension method permits important aspects of the near-tip behavior in the bilayer MMDB

geometry to be overlooked and, as a consequence, the use of this specimen will not yield specimen-independent toughness values in many common situations. Accordingly, the prime objective of the current work is specifically to investigate the extent of the region of K-dominance in this specimen geometry, both for the bilayer sample (Fig. 1a) and to a more limited extent for the sandwiched MMDB sample (Fig. 1b).

3. Numerical analysis

3.1. Finite element analysis

Finite element analysis was performed using the FEAP computer program (Zienkiewicz and Taylor, 1987) on a half-sample utilizing the line of symmetry midway between the inner loading points. A typical mesh of the bilayer sample contained roughly 10,000 nodes and a mesh of the sandwiched sample contained roughly 12,000 nodes; a simplified schematic illustration is shown in Fig. 3. In order for the model to capture the singular behavior of the interface crack, meshing in the region of the crack tip was very fine; typically, the smallest elements were of the order of $h/100{,}000$. This degree of mesh refinement was used to ensure that there were at least five rings of elements within the region of K-dominance.

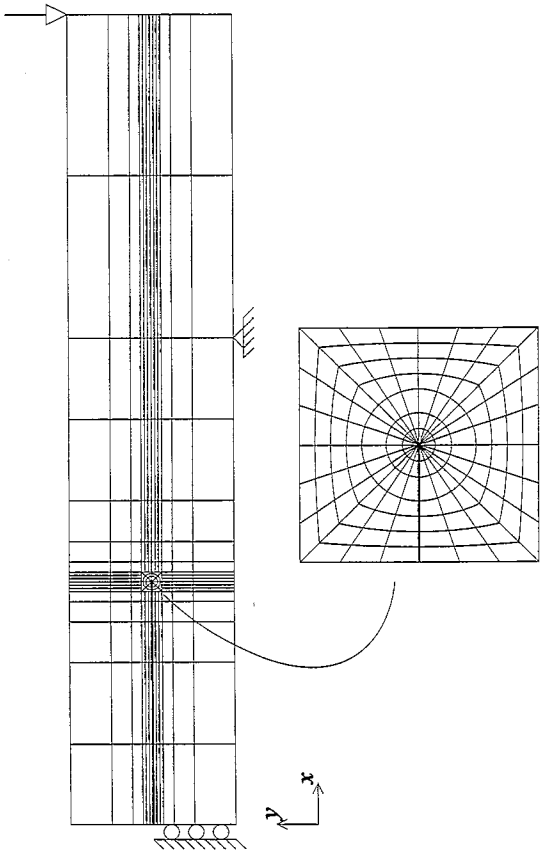

Fig. 3. Schematic illustration of the finite element mesh used for the MMDB sample, with a higher magnification view of the region near the crack tip.

The meshing at the tip of the crack (the detail in Fig. 3) consisted of twelve singular 6-node triangular elements arranged in a circle (Stern and Becker, 1978; Stern, 1979). Although these elements can reproduce the $r^{-1/2}$ singularity in the stresses found near crack tips in monolithic solids, due to elastic mismatch effects, they do not provide the exact singularity for the field around an interface crack. However, when compared to quadratic triangular elements, the singular elements were found to improve the form of the solution in the elements *surrounding* the crack tip. The remainder of the geometry was modeled using 9-node plane-strain linear-elastic isoparametric elements.

3.2. Specimen calibration

A change in compliance method was employed to calculate the value of the steady-state strain-energy release rate G_{ss}. Linear elastic solutions for G yield:

$$G = \frac{F^2}{2b}\frac{\partial C}{\partial a} = \frac{F}{2b}\frac{\partial \delta}{\partial a} \approx \frac{F}{2b}\frac{\Delta \delta}{\Delta a}, \tag{8}$$

where F is the applied load, C is the sample compliance, b is the sample thickness, a is the crack length and δ the displacement at the point of loading. Two finite element analyses were performed on samples with differing crack lengths ($\Delta a/h \sim 0.05$) and the difference in the load-point deflections were used in Eq. (8).

It is important to note that the application of a point load to the finite element model results in localized deformation in the region neighboring the contact point (due to the singularity in the stresses predicted by the theory of linear elasticity). How-

ever, since Eq. (8) depends only on the *difference* between the load point displacements corresponding to two crack lengths, the local effects of the point load are not important.

Although Eq. (8) provides a means to compute the strain-energy release rates for this sample, calculation of the interface stress intensities requires a more detailed analysis of the finite element results, specifically in the use of the finite element stresses near the tip to calculate the best fit value of the interface stress intensity. A provisional K-field prediction for the tensile-opening stresses, σ_{yy}^{K} was determined through Eq. (2) (excluding the higher order terms) and a residual R was calculated using nodal projections of the finite element stress components σ_{yy}^{fem}, viz.

$$R = \sum_{i=M}^{M+N} \left(\sigma_{yy,i}^{\text{fem}} - \sigma_{yy,i}^{K}\right)^2. \tag{9}$$

R was formed over a series of nodes ($i = M$ to $M+N$) and was minimized over a range of interface stress intensities to yield the best fit, $\boldsymbol{K}_{\text{fit}}$. Clearly for this procedure to yield accurate values for the interface stress intensity factor, i.e. for $\boldsymbol{K}_{\text{fit}}$ to be equal to $\boldsymbol{K}$ for this sample geometry, the nodes M to $M+N$ must lie within the region of K-dominance. The nodes used in this study were those in the finite elements arranged in a ring spaced two elements away from the crack tip and excluding the elements along the crack face. The omission of the crack tip and crack flank elements helped in limiting the influence of the numerical errors in the finite element calculation on the value of $\boldsymbol{K}_{\text{fit}}$. It should be emphasized that this method, rather than a course-mesh method such as virtual crack extension, was utilized because it allows examination of the details of the crack-tip stress state, specifically, K-dominance. (As shown below, the computed $\boldsymbol{K}_{\text{fit}}$ values were found to be virtually identical to previous calculations using other methods.)

This procedure was followed using the tensile-opening yy-stresses but could, in principle, have been performed using any of the components of stress, strain, or displacement, given the appropriate knowledge of the analytical solution. However, since beam theory predicts bending will cause xx-stresses and x- and y-displacements everywhere in the sample and since the behavior of the singular region had to be distinguished from that of the sample *en masse*, these were considered to be less appropriate choices in the data reduction scheme. By contrast, there are no xy- or yy-stresses due to bending, thus making it easier to analyze the field near the crack tip.

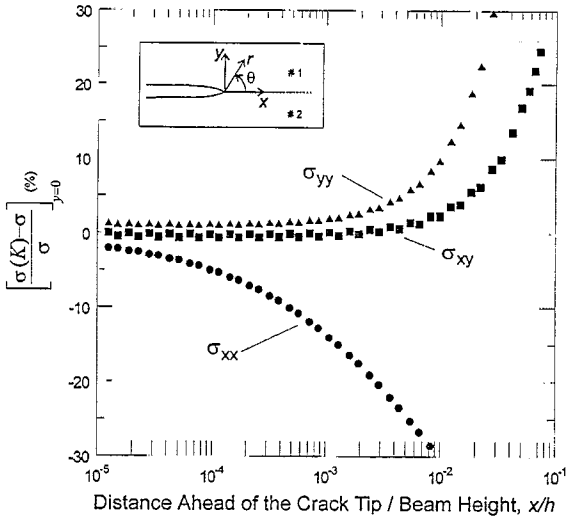

Fig. 4. Deviation of the stress components σ_{xx}, σ_{xy} and σ_{yy} computed by finite element analysis from the K-field values with normalized distance ahead of the crack tip along the interface, x/h, for the bilayer sample. Solutions for $h_1/h = 0.5$, $h = 1$, with $E_1 = E_2 = 1$ and $\nu_1 = \nu_2 = 0.3$.

3.3. Determination of K-dominance

The stresses computed in the finite element analysis were employed with the complex interface stress-intensity factor $\boldsymbol{K}$ (e.g., the $\boldsymbol{K}_{\text{fit}}$ values calculated in Section 3.2) to calculate the size of the region of K-dominance. The leading term of Eq. (2) was used with $\boldsymbol{K}$ to calculate the values of the stresses around the interface crack predicted by LEFM, the K-field. Such an analysis of the crack-tip field is shown in Fig. 4, where the deviations of the different stress components from those of the K-field are displayed for this sample as a function of distance x directly ahead of the crack tip.

Closest to the crack tip, there is little deviation between the K-field and the finite element stresses. With increasing distance from the crack tip, the xy-

and yy-stresses continue to exhibit a region over which there is little difference between the K-field and the finite element stresses (approximating the full-series values for the stresses); this represents the region of K-dominance. However, with progressively increasing distances from the crack tip, the difference between the K-field stresses and the finite element stresses becomes larger, thus defining the limit of K-dominance. It is interesting to note that the xx-stresses more quickly deviate from the singular form, only converging to the K-field values much closer to the crack tip.

In the current work, we define the region of K-dominance in terms of the yy-component of stress, σ_{yy}, as this stress component is invariably of prime importance in the propagation of cracks along the interface. The distance along the interface ahead of the crack tip at which the K-field and the finite element values of σ_{yy} differed by more than 5% was used as an operational definition of the size, r_K, of the K-dominant region. Although 5% is somewhat arbitrary, it proved to be sufficiently larger than the computational errors in the FEM analysis such that the results are unambiguous. We note, however, that using the xx-stresses to determine r_K would have led to much smaller values of r_K (by some two orders of magnitude). This may be due to the far-field bending xx-stresses present in the MMDB sample.

4. Results

4.1. The bilayer MMDB specimen

Finite element analyses and subsequent stress intensity calibrations were performed for a series of bilayer MMDB (Fig. 1a) specimens with differing layer heights ($0.05 \le h_1/h \le 0.5$, $h_1 + h_2 = 1$) but identical elastic properties ($E_2/E_1 = 1$, $\nu_1 = \nu_2 = 0.3$). A comparison of the finite element and K-field values of the σ_{yy} stresses in Fig. 5a (and later in Fig. 7a) reveals a small plateau difference ($\sim 1\%$) at $x/h < 10^{-4}$, within the region of K-dominance. This difference is largely due to the fact that the stress-intensity factor was obtained using a fit over a large range of θ; whereas the data in Fig. 5a are obtained considering only the stresses along the interface i.e. at $\theta = 0$. Indeed, had a different angle been chosen,

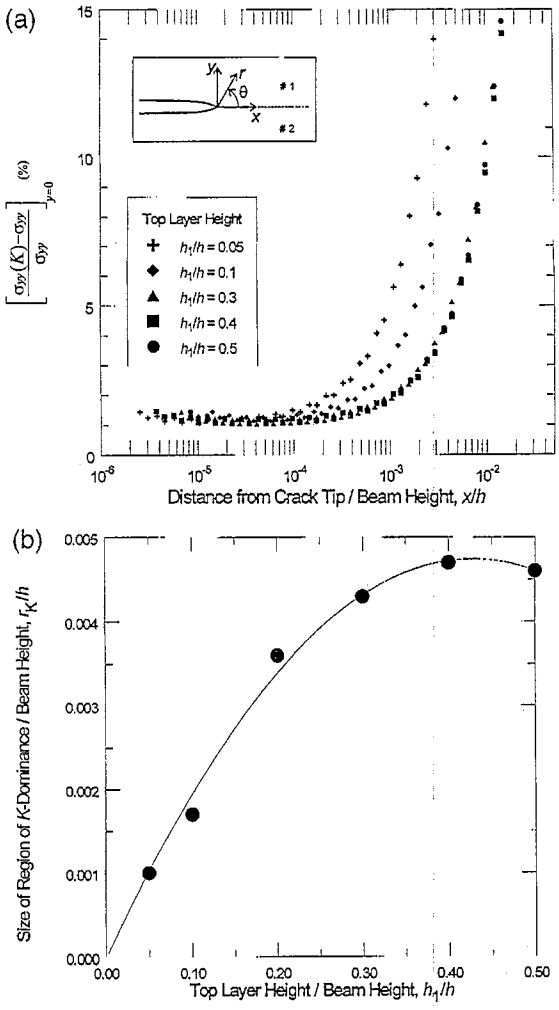

Fig. 5. (a) Deviation of the tensile-opening stress components, σ_{yy}, from the K-field as a function of normalized distance ahead of the crack tip along the interface, x/h, for a bilayer MMDB sample with $E_2/E_1 = 1$ and $\nu_1 = \nu_2 = 0.3$, where the ratio of the height of the top layer to the overall specimen height, h_1/h is varied from 0.05 to 0.5 and (b) the corresponding effect of the top layer height, h_1, on the size of the region of K-dominance, r_K.

a different plateau error would be seen; furthermore, a refinement of the mesh in the θ-direction would decrease the magnitude of this error. The use of a range of θ in the calculation of K_{fit} improved its accuracy, such that the steady-state strain-energy release rate G_{ss} determined from K_{fit} (via Eq. (4)) was found to be within 0.5% of the values calculated in the present study from Eq. (8) and the previous

results of Charalambides et al. (1989) and Suo and Hutchinson (1990) (Fig. 6). Indeed, both the strain-energy release rate G_{ss} and the reference phase angle Ψ^* computed using K_{fit} were found to be nearly identical to the previously computed values.

However as noted above, when K_{fit} (or the previous calibration for the bilayer sample) was used to calculate the K-field values of the yy-stresses, the latter were found to quickly deviate from the finite element (full-series) values with increasing distance from the tip (Figs. 5 and 7a) once $r > r_K$.

The change in the size of the region of K-dominance with the top layer thickness (h_1) is presented in Fig. 5b. Using the 5%-deviation definition given above, the extent of the K-dominant region for these homogeneous samples, r_K^H, can be seen to vary markedly with the top layer thickness, h_1. Specifically, it decreases with decreasing top layer thickness, with r_K^H/h ranging from 0.001 (for $h_1/h = 0.05$) to 0.005 (for $h_1/h = 0.4$). For small h_1, $r_K^H \sim h_1/50$; however, r_K^H is not strictly proportional to the smallest specimen dimension h_1, as there is little effect of the top layer height on r_K^H for $h_1/h \geq 0.3$.

The effects of varying the substrate stiffness are displayed in Fig. 7a, where a range of stiffnesses $0.1 \leq E_2/E_1 \leq 10$ ($\nu_1 = \nu_2 = 0.3$) is considered for $h_1/h = 0.5$. The size of the K-dominant region increases slightly with increasing substrate stiffness, with r_K/h ranging from 0.005 (for $E_2/E_1 = 0.1$) to 0.007 (for $E_2/E_1 = 10$); these results are displayed in Fig. 7b.

4.2. The sandwiched MMDB specimen

A full and detailed analysis of the corresponding geometry with the thin sandwiched interlayer (Fig. 1b), requiring exploring of a very wide array of sample dimensions and material parameters, is beyond the scope of the present study. However, to assess the effect of the interlayer on the stress-intensity factor K and on the size of the K-dominant region, a limited study of the sandwiched sample with a crack at the top interface was undertaken. For these calculations, a thin layer was sandwiched between elastically identical materials such that $h_1/h = 0.3$, $\nu_1 = \nu_2 = 0.3$ and $E_2/E_1 = 1/5$ or 10. The thickness of the sandwiched layer was varied from 0.1–20% of the total beam height.

The strain-energy release rates for the sandwiched sample are compared to G for a homogeneous bilayer ($h_1/h = 0.3$) sample in Fig. 8a. It is clear that the homogeneous solution usually underestimates the driving force for crack growth for compliant interlayers, such as for metal-bonded ceramics. The phase angles, Ψ^* (referenced to the beam height, h) for the sandwiched sample, are displayed in Fig. 8b.

Given that the size of the K-dominant region is affected by the size of the smallest specimen dimension, it may be expected that the value of r_K for the sandwiched sample will be smaller than for the bilayer sample. The results in Fig. 9 clearly show the strong effect of the interlayer size and properties on the region of K-dominance, with r_K being roughly equal to 1/10 of the interlayer height for very thin layers ($h_{sand}/h < 0.05$). The trends extending beyond $h_{sand}/h = 0.3$ are obtained by equating a sandwiched sample containing an interlayer extending over the entire substrate (i.e. such that $h_2 = 0$) and the bilayer sample with the same E_2/E_1 and h_1/h. Thus, the values of r_K for $h_{sand}/h = 0.7$ plotted in Fig. 9 are identical to those for the bilayer sample with $h_1/h = 0.3$.

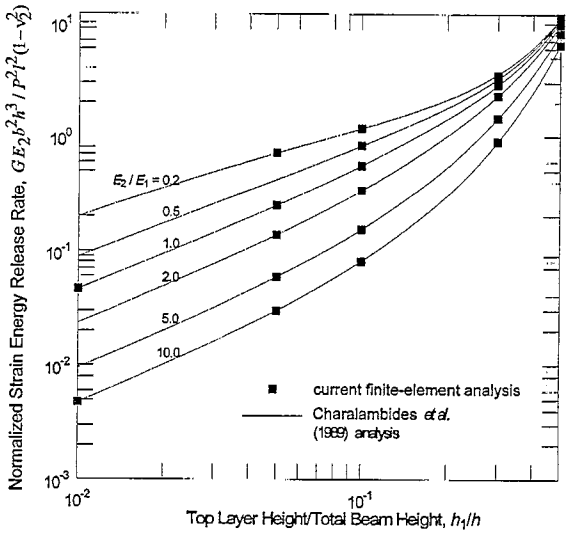

Fig. 6. Comparison of the Charalambides et al. (1989) and Suo and Hutchinson (1990) analytical predictions for the non-dimensional G_{ss} in the bilayer MMDB sample geometry with the current finite element results (shown on a log–log scale for clarity). Values for the reference phase angles Ψ^* show similar agreement with the earlier calculations of Charalambides et al. (1989).

The complex behavior of r_K displayed in Fig. 9, particularly for $E_2/E_1 = 1/5$, should be noted. First, for stiffer interlayers the situation is simpler and r_K varies monotonically between being the smaller of $h_{sand}/10$ and of r_K^H for $h_1/h = 0.3$. In contrast, for more compliant layers the limiting behaviors are

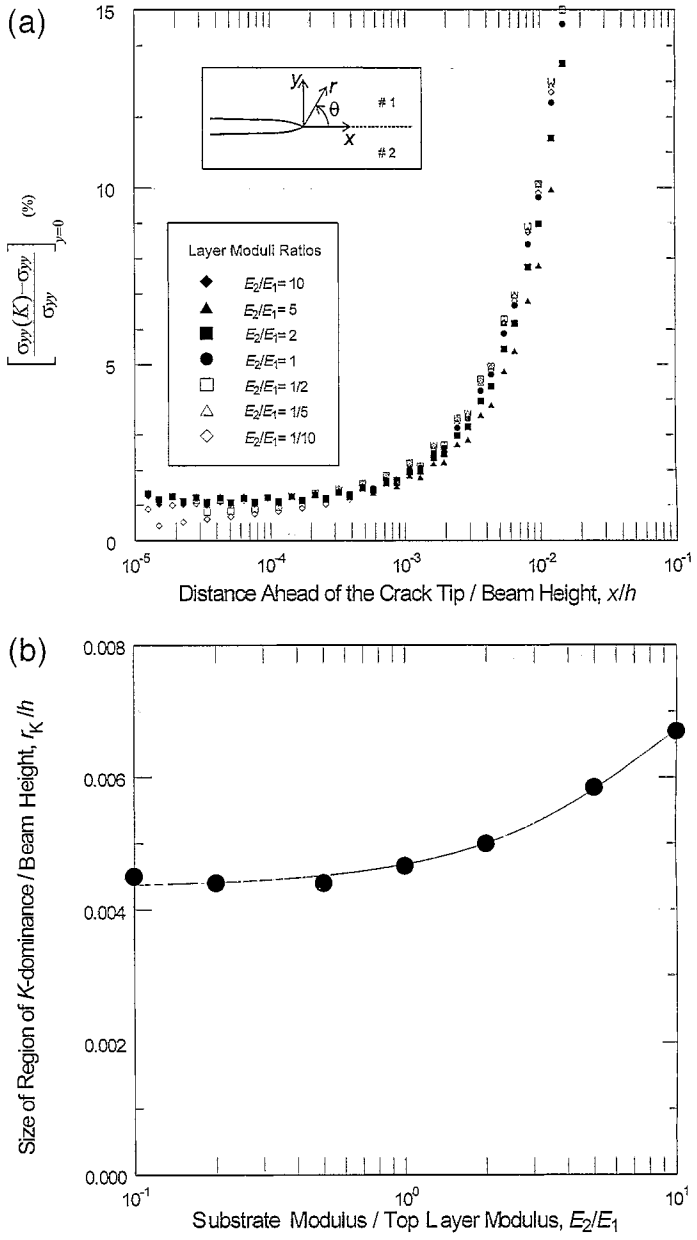

Fig. 7. (a) Deviation of the tensile-opening stress components, σ_{yy}, from the K-field as a function of normalized distance ahead of the crack tip along the interface, x/h, for a bilayer MMDB sample with $h_1/h = 0.5$, where the ratio of the substrate layer moduli to top layer moduli, E_2/E_1, is varied from 0.1 to 10 ($\nu_1 = \nu_2 = 0.3$) and (b) the corresponding effect of the modulus ratio, E_2/E_1, on the size of the region of K-dominance, r_K.

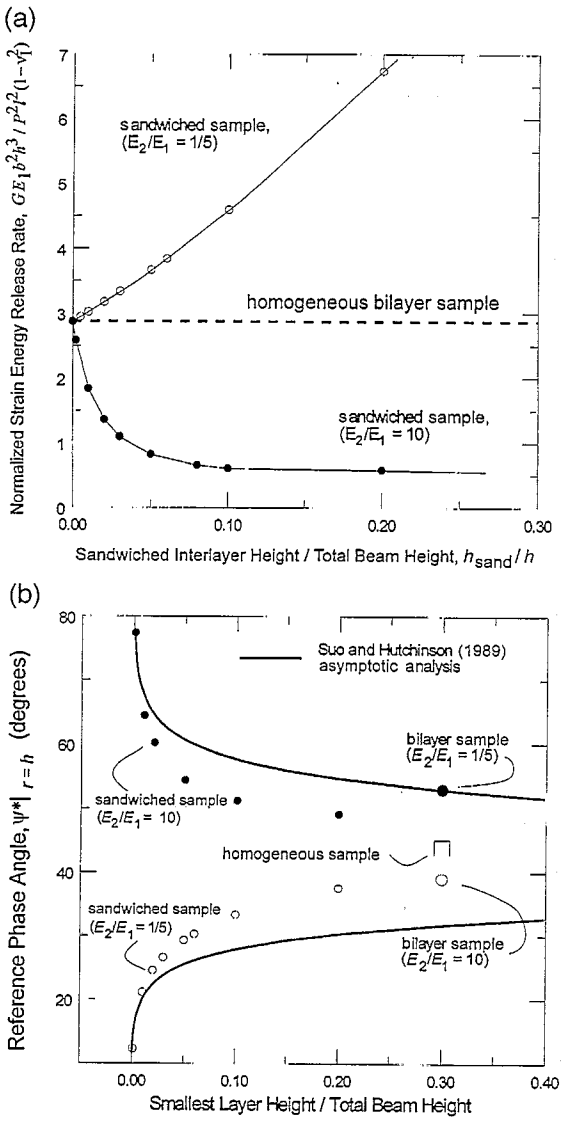

Fig. 8. (a) Comparison of the current finite element calculation of the non-dimensional strain-energy release rates for the sandwiched MMDB sample (with $E_2/E_1 = 1/5$ and 10) with G_{ss} for a homogeneous sample (both samples with $h_1/h = 0.3$). (b) Comparison of the reference phase angles Ψ^* for the sandwiched MMDB sample geometry with the asymptotic calculations of Suo and Hutchinson (1989). Also shown are data points for the homogeneous and bilayer (with $E_2/E_1 = 1/5$ and 10) samples.

similar, but for intermediate values of h_{sand}, r_K is larger than r_K^H. This is due to a change in the form of the deviation of the stresses from the K-field values. Unlike the bilayer samples (Figs. 5 and 7a), the stresses do not deviate from the K-field monotonically for intermediate layer heights ($h_{sand}/h \sim 5$–10%). For example, for $E_2/E_1 = 1/5$ and $h_{sand}/h = 0.05$ the error in the K-field oscillates in sign with increasing r up to $r/h = 10^{-3}$; however, the magnitude of the oscillation is less that the threshold 5% value. It is this change in the sign of the deviation that leads to a large calculated region of K-dominance.

It is clear that for very thin interlayers ($h_{sand}/h < 0.02$), which have been commonly used in bimaterial studies (Table 1), the size of the K-dominance zone in the sandwiched sample is bounded by that of the homogeneous sample. Thus, r_K^H can be used as an approximation of r_K in the sandwiched MMDB sample; however, $h_{sand}/10$ may be a more accurate value of r_K with any non-vanishing modulus mismatch.

5. Discussion

5.1. The bilayer MMDB specimen

The calculations for the bilayer mixed-mode delaminating beam specimen described above clearly

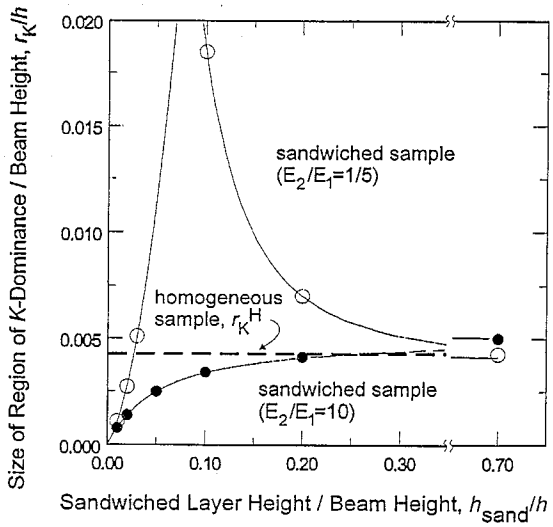

Fig. 9. The effect of the sandwiched interlayer height, h_{sand}, on the size of the region of K-dominance, r_K, for the sandwiched interlayer sample with $h_1/h = 0.3$, $E_2/E_1 = 10$ and 1/5 and $\nu_1 = \nu_2 = 0.3$. Results for the homogeneous sample with $h_1/h = 0.3$ are included for comparison (dashed line).

Table 1

Material combination: substrate/layer(s)	Ref.	Beam height, h (mm)	Sandwich layer height, h_{sand} (μm)	Interpenetration zone size, r_{int} (nm)	Plastic zone size, r_p^{∞} (μm)	K-dominance zone size, r_K (μm)	r_p^{∞}/r_K
SiC/SiC	Phillipps et al. (1993)	6	—	~ 0	~ 0	27	~ 0
Al/PMMA	Charalambides et al. (1989, 1990)	6	—	0.00004	54	72	0.75
Ti(Ta)/sapphire	Bartlett and Evans (1993)	1.25	—	0.001	4.7	3.8	1.2
Ti-6Al-4V/Ti	Howard and Clyne (1993)	2.8	—	~ 0	99	26	3.8
$Al_2O_3/Ti/Al_2O_3$	Wang and Gerberich (1993)	6	6–127	0.4	53	27 [a]	2
Sapphire/Au/sapphire	Reimanis et al. (1991)	4.6	10–100	0.14	603	20 [a]	30
Sapphire/Cu/sapphire	Reimanis et al. (1993)	4.3	25–130	4.3	2000	19 [a]	105
$Al_2O_3/Al/Al_2O_3/Al$/Sapphire	Shaw et al. (1994)	3.5	40–250	70	3500	16 [a]	219

[a] The estimate based on a homogeneous beam, r_K^H, has been used.

indicate that for a wide range of layer heights ($0.05 \leq h_1/h \leq 0.5$) and layer moduli ($0.1 \leq E_2/E_1 \leq 10$), the region of K-dominance at the crack tip in this geometry is extremely limited; it is at least an order of magnitude smaller than the $\sim 1/10$ of the characteristic specimen dimension commonly assumed for other fracture-mechanics samples. Indeed, for the range of h_1/h and E_2/E_1 studied, estimates for the extent of r_K can be less than $1/1000$ of the beam height, and rarely exceed $1/100$ of this dimension.

These trends indicate that interfacial fracture toughness data measured with these specimens could be inherently non-conservative. This can be understood from the similitude principle: the near-tip state of stress for cracks in different bodies will be accurately characterized by $\boldsymbol{K}$ (or equivalently G and Ψ^*). The data in Fig. 4 clearly show that the singular $\boldsymbol{K}$ field over-estimates the elastic yy-stresses in this specimen geometry at distances beyond r_K. For example, if an RKR-type criterion, involving a critical fracture yy-stress being exceeded over some characteristic dimension (Ritchie et al., 1973), is assumed to describe the local fracture behavior of a brittle solid in this geometry, then the actual stresses ahead of the crack tip will be lower than those predicted by the singular LEFM field; this, in turn, means that for finite samples higher loads must be applied to cause failure, resulting in experimental values of G_c being higher than the actual critical value. However, as shown in Fig. 4, σ_{xx} is actually larger than the K-field value, which could, for some damage mechanisms, offset the effect of σ_{yy} being smaller; in particular, at small θ the actual mean stress would also be somewhat larger than expected.

In addition, for stress intensities measured at instability or prior to subcritical crack extension to be geometry independent, it is imperative that the region of K-dominance extends beyond the dimensions in which the assumptions of linear elasticity are violated. For bilayer interface samples, these latter dimensions specifically involve regions of crack-surface interpenetration and more importantly plastic deformation.

For the material combinations and phase angles considered here, the displacement equations for the crack flanks predict interpenetration to occur over dimensions of the order of $r_{int}/h \sim 10^{-11}$–10^{-6}, Table 1. As this is often nearly atomic dimensions for a laboratory sample and always many orders of magnitude smaller than the region of K-dominance, interpenetration is clearly not an issue with this geometry.

Of greater importance is the dimension associated with constitutive nonlinearity (e.g., plasticity). Clearly for any linear-elastic analysis of a crack geometry to be valid, the size of the inelastic zone must be small compared to the specimen dimensions and crack size, $r_p \ll a, h$. Moreover, as stated previously, to yield meaningful results based on such linear-elastic solutions, the SSY condition must be met, with the nonlinear zone being small compared to the extent of K-dominance i.e. $r_p \ll r_K$. Since it has been shown that the K-dominant region is less then $1/100$ of the specimen dimensions in the bilayer MMDB sample, the use of this geometry is likely to be highly questionable for many common ceramic/metal combinations and typical specimen dimensions.

A review of the literature yields many examples of the use of the bilayer MMDB geometry to study mixed-mode bimaterial interfacial fracture behavior (Charalambides et al., 1989; Bartlett and Evans, 1993; Howard and Clyne, 1993; Phillipps et al., 1993). The sizes of the samples typically used involve beam heights of $h = 1$–6 mm for a wide range of bimaterial pairs (Table 1).

For comparison, the plastic zone size was calculated using Eq. (6). Although this analysis is strictly valid only for an infinite body, r_p^∞ should serve as a suitable approximation for r_p. A comparison of computed values of r_K with the mixed-mode plastic-zone size, r_p, is made for these selected examples in Table 1. For the Ti(Ta)/sapphire alloy and Ti-6Al-4V/Ti systems examined, it is clear that the actual plastic zones at failure extend over dimensions from the crack tip far in excess of the zone of K-dominance; indeed, even with the Al/PMMA system, the experiments reported do not meet the criterion of $r_p \ll r_K$. Since it is unclear how the stress, strain and displacement fields surrounding the crack tip during the fracture event would scale with the applied stress intensities, it is doubtful that an appropriate characterizing parameter can be obtained accurately through the use of LEFM. However, LEFM calibrations for the bilayer MMDB sample were used in the analyses for all the results cited; accordingly, it is apparent

that the toughness values reported in these studies are specimen-dependent, i.e. not the limiting SSY fracture toughnesses. Clearly, with such a highly restricted region of K-dominance in this specimen, use of the bilayer mixed-mode delaminating beam geometry for further studies should be undertaken with some caution.

5.2. The sandwiched MMDB specimen

The analysis of the MMDB specimen with a sandwiched layer yielded results that depend appreciably on the modulus ratio, E_2/E_1, and on the size of the interlayer, h_{sand}. This work illustrates several interesting features of interface fracture mechanics for layered structures that also have applicability to some other geometries.

Insight into the mechanics underlying the behavior of the sandwiched MMDB sample can be gained by comparing it to the homogeneous bilayer sample. In the asymptotic thin-layer limit, the strain-energy release rate for the sandwiched sample, G, is equal to that for the homogeneous sample. The results in Fig. 8a confirm that as $h_{sand} \to 0$, the strain-energy release rate for the sandwiched sample approaches that of the bilayer sample; however, for layers that are as thin as $h/50$, the strain-energy release rate can be drastically different from that of the homogeneous sample. In addition, the reference phase angle [2] is accurately described by the asymptotic analysis only for $h_{sand}/h \leq 100$ (Fig. 8b), an unexpectedly small value. Again, this is a consequence of the limited region of K-dominance in the homogeneous bilayer sample ($r_K^H/h \leq 0.005$, Fig. 5b) which leads to these restrictions on the application of this analysis for the sandwiched sample.

For thicker layers, this asymptotic situation does not apply, but there is a region of interfacial K-dominance which, if $E_2/E_1 > 1$, is smaller than r_K^H and for smaller layers is $\sim h_{sand}/10$. The K-dominant region is larger for $E_2/E_1 < 1$; in certain regions it approaches $h_{sand}/5$ and can even exceed r_K^H, (Fig. 9). Furthermore, the corrections for G and Ψ^* are smaller where the layer is compliant than for the case where the sandwiched layer is stiffer, (Fig. 8a and b), for which the errors are appreciable with h_{sand} exceeding only 1% of the beam height. Comparison of results from Fig. 8a and b show that when $h_{sand}/h > 0.05$ and $E_2 \neq E_1$, neither the asymptotic sandwiched nor the bilayer approximation gives a satisfactory approximation for G.

When plasticity occurs at the crack tip, geometry insensitive SSY toughness measurements analyzable within the context of LEFM are expected when $r_p \ll r_K$. For sandwich samples, two limiting conditions can be envisaged for interface fracture when the interlayer is more ductile. First, if the plastic zone is embedded within the interfacial K-dominant region and is much smaller than the sandwiched layer thickness, so as to be largely unconstrained by the opposite interface, then the *SSY interface toughness* can be derived. This requires that $r_p \ll (r_K, h_{sand})$ i.e. that:

$$r_p^\infty/h_{sand} \ll (r_K/h_{sand}, 1). \tag{10}$$

The condition for this can be seen graphically by renormalizing the plot for r_K, Fig. 9, to the interlayer heights as shown in Fig. 10 where r_K/h_{sand} is plotted against h_{sand}/h. This SSY interface fracture region can be visualized as a region in an analogous plot of r_p/h_{sand} versus h_{sand}/h. The acceptable range is under the pertinent r_K/h_{sand} curve (the lower part of Fig. 10), satisfying both conditions unless $E_2/E_1 \sim 1$; in this case, $r_K \sim r_K^H$ and the region of $r_p^\infty/h_{sand} > 1$ is inappropriate. As emphasized earlier, the computation of G and Ψ^* can be accomplished from published analyses if the layer is thin enough to be in the asymptotic limit, i.e. $r_K^H/h_{sand} \gg 1$, requiring $h_{sand}/h \ll 0.005$ (the left side of Fig. 10). Then, in addition, the reference plastic phase angle, ξ, follows directly from Eq. (7). For thicker interlayers, this SSY condition can be met, but G, Ψ^* and ξ must be computed explicitly to avoid errors similar to those depicted in Fig. 8.

The second limiting condition occurs when the entire thickness of interlayer becomes plastic in a region near the crack-tip. Then it is widely expected (Reimanis et al., 1991; Wang and Gerberich, 1993) that G_c will scale with h_{sand}, but these toughness

[2] Note that the rapid change in reference phase angle with layer height is a result of using h for the reference distance; if the reference distance were set to h_{sand}, the Suo and Hutchinson (1989) analysis would result in a constant shift in the phase angle of $-8.4°$ or $3.3°$ from the homogeneous case (for $E_2/E_1 = 10$ or $1/5$).

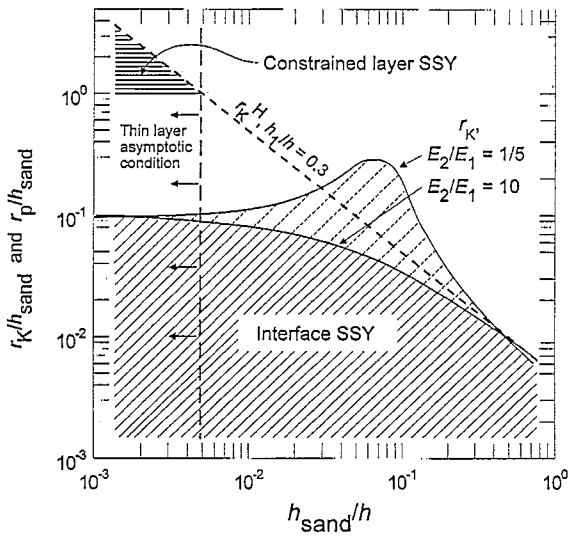

Fig. 10. Plot of normalized plastic zone size, r_p versus normalized sandwiched interlayer height, h_{sand}, on which conditions are delineated for two different types of small scale yielding. The lower condition giving the interface toughness with an unconstrained plastic zone, is bounded by the size of the interface K-dominance zone, r_K which depends on modulus mismatch. The constrained SSY condition involving a fully plastic layer is limited by the homogeneous K-dominance region, r_K^H.

values can be used in various other geometries if the interlayer is entirely within the homogeneous K-dominant region. An approximate condition for this is:

$$1 \ll r_p/h_{sand} \ll r_K^H/h_{sand} \tag{11}$$

The resulting toughness can be termed the *constrained layer SSY interface toughness*. Thus, the plastic deformation has eliminated the elastic interface K-dominant region, but the interlayer is within the homogeneous K-field. This region is located graphically by a small triangular area in the upper left of Fig. 10.

Unfortunately, computing the extent of the plastic zone in this sample is complicated by the highly constrained state of the sandwiched interlayer. It is clear that for $r_p^\infty > h_{sand}$, the plastic zone will be limited to a distance h_{sand} perpendicular to the crack plane, although there will be no such restriction in the direction ahead of the crack tip. Plastic-zone size calculations for a mode-I crack in a constrained ductile layer (Varias et al., 1991) show a reduction in r_p by a factor of 5 for large plastic zones, $r_p > h_{sand}$ when compared to estimates for a similar crack in an unconstrained metal, where $r_p^\infty \approx K_I^2/2\pi\sigma_y^2$. An analysis of the effect of such constraint on a mixed-mode interface crack has not been performed for plastic-zone sizes on the order of the sandwiched layer thickness, although it is reasonable to infer that a similar reduction in the amount of plasticity will occur.

In the constrained layer SSY regime, the calculation of G using the asymptotic elastic approximation is quite good regardless of layer compliance, analogous to the limit in Fig. 8a. Although no convention for associating the phase angle with the thickness dependent toughness has yet been widely adopted, the use of the elastic Ψ^* and Eq. (7) would yield an unambiguous value of the reference plastic phase angle, ξ, that pertains near the elastic–plastic boundary ahead of the crack. This allows for the investigation of thickness dependent interface toughnesses for various phase angles.

Perhaps more than as a bilayer specimen, the MMDB test geometry has been widely used with a sandwiched interlayer in fracture and crack-growth studies (Reimanis et al., 1991, 1993; Wang and Gerberich, 1993; Shaw et al., 1994; Ritter et al., 1994). To assess whether the LEFM crack-tip field solutions were valid for such use, it is again necessary to compare the extent of K-dominance with the plastic-zone sizes as is done for several ceramic-metal interfaces (Table 1). The calculations in Shih (1991) of the plastic-zone size, r_p^∞ in Eq. (6), for a mixed-mode loading of a crack between two infinite bodies were used presently to assess the applicability of the sandwiched specimen geometry, with the comment that for plastic-zone sizes on the order of h_{sand}, the actual amount of plasticity will be less than represented here.

Although some experiments contained interlayers that were embedded within a homogeneous K-field (i.e. $h_{sand}/h < 0.005$), it is clear that none meet the bimaterial SSY criteria, $r_p \ll r_K \sim h_{sand}/10$. Indeed, only the data using the thinnest layers in the sapphire/Au, sapphire/Cu and Al_2O_3/Ti studies can be interpreted as a constrained layer SSY interface toughness, while no work cited measured the SSY interface toughness. In addition, each of the studies

cited utilized a range of interlayer heights that exceeded the constrained layer SSY criteria, $h_{sand} \ll r_K^H$. Clearly, a reevaluation of the role of the sandwiched MMDB sample, analyzed using LEFM, is required for future studies of bimaterial interfaces and layered materials.

5.3. Concluding remarks

It is apparent that the region of K-dominance in the MMDB specimen is far smaller than that found for other commonly used fracture-mechanics test geometries (Fig. 2). This evidently arises from the thin membered geometry in which the xx-stress is the only non-zero, far-field stress component to be converted into the singular K-field. In addition, it should be remarked that the analyses leading to these conclusions are based largely on discrepancies in σ_{yy}. The σ_{xx} values are erroneous at much smaller dimensions, and using the next order term, the 'T-stresses', would only be of limited help. However, the reasonable convergence of G and especially Ψ^* to asymptotic values when $h_{sand} < r_K^H$, Fig. 8, suggests that basing r_K on the yy-stresses is useful for many issues.

Similar problems of very small regions of K-dominance can be expected to apply to two other well-studied interfacial fracture geometries for which simple analytic solutions for G can be derived from beam theory. One is the thin double-cantilever beam (DCB) sample, which has been used extensively for interfacial fracture resistance measurements e.g., Oh et al. (1987) and Cannon et al. (1991). Here, similar limitations as those indicated in Figs. 5–9 on the size of the r_K and the magnitude of corrections for the G and Ψ^* may be expected to apply. Indeed, although values of r_K^H (and therefore the critical h_{sand}/h for the asymptotic analysis to apply) computed for $h_1/h = 0.5$ would be more nearly pertinent for the symmetrical DCB samples, Fig. 5b shows that r_K^H is little different than r_K^H for $h_1/h = 0.3$, the spacing used to study the sandwiched MMDB geometry. A second relevant geometry involves several of the thin film cracking and delamination problems which have been analyzed, e.g., Hutchinson and Suo (1992), where again the results in Fig. 5 for small h_1 should apply directly for the case of delaminating films under residual tension; this would imply that $r_K \approx h_{film}/50$.

6. Summary

The results of linear-elastic finite element calculations on the bilayer mixed-mode delaminating beam (MMDB or 'UCSB') geometry were found to confirm the steady-state interface stress intensity, strain-energy release rate and phase angle solutions derived previously. However, the present analysis shows that the size of the region of K-dominance near the crack tip, r_K, in the bilayer version of this geometry only extends over radial distances from the tip of $1/100$ to $1/1000$ of the total specimen height. Moreover, for the sandwiched interlayer version, the value of r_K is even smaller; for an interlayer $1/20$ of the beam height, r_K is of the order of $1/10$ of the interlayer height. Accordingly, for a linear-elastic fracture mechanics analysis to be valid for the bimaterial specimen geometry, any extent of local plasticity must be much smaller than $\sim 1/200$ of the beam height. For the sandwich geometries, the plastic zone should be much less than $1/200$ of the beam height to satisfy the constrained layer small scale yielding limit, and much less that $1/10$ of the interlayer height to satisfy the more stringent SSY interface toughness limit. It is found that for the majority of common metal/ceramic systems reported in the literature that have been analyzed using MMDB specimens, the extent of plastic-zone readily exceeds these regions of K-dominance; thus the utility of LEFM-based analysis with this sample for measuring geometrically insensitive toughnesses becomes highly questionable.

Acknowledgements

This work was supported by the Director, Office of Energy Research, Office of Basic Energy Sciences, Materials Sciences Division of the U.S. Department of Energy under Contract No. DE-AC03-76SF00098.

Appendix A

The equation for the stresses around an interface crack (Eq. (2)) include functions of ε and θ, Σ_{jk}^{I} and Σ_{jk}^{II} (Rice et al., 1990). For $\theta = 0$ to π:

$$\Sigma_{rr}^{I} = \frac{-\sinh[\varepsilon(\pi-\theta)]\cos(\frac{3}{2}\theta)}{\cosh(\pi\varepsilon)} + \frac{e^{-\varepsilon(\pi-\theta)}}{\cosh(\pi\varepsilon)}\cos\left(\frac{\theta}{2}\right)\left(1+\sin^2\left(\frac{\theta}{2}\right)+\varepsilon\sin(\theta)\right)$$

$$\Sigma_{\theta\theta}^{I} = \frac{\sinh[\varepsilon(\pi-\theta)]\cos\left(\frac{3}{2}\theta\right)}{\cosh(\pi\varepsilon)} + \frac{e^{-\varepsilon(\pi-\theta)}}{\cosh(\pi\varepsilon)}\cos\left(\frac{\theta}{2}\right)\left(\cos^2\left(\frac{\theta}{2}\right)-\varepsilon\sin(\theta)\right)$$

$$\Sigma_{r\theta}^{I} = \frac{\sinh[\varepsilon(\pi-\theta)]\sin\left(\frac{3}{2}\theta\right)}{\cosh(\pi\varepsilon)} + \frac{e^{-\varepsilon(\pi-\theta)}}{\cosh(\pi\varepsilon)}\sin\left(\frac{\theta}{2}\right)\left(\cos^2\left(\frac{\theta}{2}\right)-\varepsilon\sin(\theta)\right)$$

$$\Sigma_{rr}^{II} = \frac{\cosh[\varepsilon(\pi-\theta)]\sin\left(\frac{3}{2}\theta\right)}{\cosh(\pi\varepsilon)} - \frac{e^{-\varepsilon(\pi-\theta)}}{\cosh(\pi\varepsilon)}\sin\left(\frac{\theta}{2}\right)\left(1+\cos^2\left(\frac{\theta}{2}\right)-\varepsilon\sin(\theta)\right)$$

$$\Sigma_{\theta\theta}^{II} = \frac{-\cosh[\varepsilon(\pi-\theta)]\sin\left(\frac{3}{2}\theta\right)}{\cosh(\pi\varepsilon)} - \frac{e^{-\varepsilon(\pi-\theta)}}{\cosh(\pi\varepsilon)}\sin\left(\frac{\theta}{2}\right)\left(\sin^2\left(\frac{\theta}{2}\right)+\varepsilon\sin(\theta)\right)$$

$$\Sigma_{r\theta}^{II} = \frac{\cosh[\varepsilon(\pi-\theta)]\cos\left(\frac{3}{2}\theta\right)}{\cosh(\pi\varepsilon)} + \frac{e^{-\varepsilon(\pi-\theta)}}{\cosh(\pi\varepsilon)}\cos\left(\frac{\theta}{2}\right)\left(\sin^2\left(\frac{\theta}{2}\right)-\varepsilon\sin(\theta)\right)$$

For $\theta = \pi$ to 0, replace π with $-\pi$.

References

Bartlett, A., Evans, A.G., 1993. The effect of reaction products on the fracture resistance of a metal/ceramic interface. Acta Metall. Mater. 41, 497–504.

Cannon, R.M., Dalgleish, B.J., Dauskardt, R.H., Oh, T.S., Ritchie, R.O., 1991. Cyclic fatigue-crack propagation along ceramic/metal interfaces. Acta Metall. Mater. 39, 2145–2156.

Charalambides, P.G., Cao, H.C., Lund, J., Evans, A.G., 1990. Development of a test method for measuring the mixed mode fracture resistance of bimaterial interfaces. Mech. Mater. 8, 269–283.

Charalambides, P.G., Lund, J., Evans, A.G., McMeeking, R.M., 1989. A test specimen for determining the fracture resistance of bimaterial interfaces. J. Appl. Mech. 65, 77–82.

Comninou, M., 1990. An overview of interface cracks. Eng. Fract. Mech. 37, 197–208.

Drory, M.D., Thouless, M.D., Evans, A.G., 1988. On the decohesion of thin films. Acta Metall. 36, 2019–2028.

Dundurs, J.J., 1969. Edge-bonded dissimilar orthogonal elastic wedges under normal and shear loading. J. Appl. Mech. 36, 650–652.

England, A.H., 1965. A crack between dissimilar media. J. Appl. Mech. 15, 400–402.

Evans, A.G., Rühle, M., Dalgleish, B.J., Thouless, M.D., 1987. On prevalent whisker toughening mechanisms in ceramics. In: Advanced Structural Ceramics, M.R.S, Symposium Proceedings, vol. 78. Materials Research Society, Pittsburgh, PA, pp. 259–271.

Gu, P., 1993. Multilayer material with an interface crack. J. Appl. Mech. 60, 1052–1054.

Howard, S.J., Clyne, T.W., 1993. Surface preparation of titanium for vacuum plasma spraying and its effect on substrate/coating interfacial fracture toughness. Composites 24, 603–610.

Hutchinson, J.W., Suo, Z., 1992. Mixed mode cracking in layered materials. Adv. Appl. Mech. 29, 63–191.

Knott, J.F., 1973. Fundamentals of Fracture Mechanics. Butterworth, London, UK.

Matos, P.P.L., McMeeking, R.M., Charalambides, P.G., Drory, M.D., 1989. A method for calculating stress intensities in bimaterial fracture. Int. J. Fract. 40, 235–254.

Oh, T.S., Cannon, R.M., Ritchie, R.O., 1987. Subcritical crack growth along ceramic-metal interfaces. J. Am. Ceram. Soc. 70, C352–C355.

O'Dowd, N.P., Shih, C.F., Stout, M.G., 1992. Test geometries for measuring interfacial fracture toughness. Int. J. Solids Struct. 29, 571–589.

Phillipps, A.J., Clegg, W.J., Clyne, T.W., 1993. Fracture behavior of ceramic laminates in bending. II. Comparison of model prediction with experimental data. Acta Metall. Mater. 41, 819–827.

Reimanis, I.E., Dalgleish, B.J., Trumble, K.P., 1993. Fracture at Cu/sapphire interfaces. Ceram. Trans. 35, 219–228.

Reimanis, I.E., Dalgleish, B.J., Evans, A.G., 1991. The fracture resistance of a model metal/ceramic interface. Acta Metall. Mater. 39, 3133–3141.

Rice, J.R., 1974. Limitations to the small scale yielding approxi-

mation for crack tip plasticity. J. Mech. Phys. Solids 22, 17–26.

Rice, J.R., 1988. Elastic fracture mechanics concepts for interfacial cracks. J. Appl. Mech. 55, 98–103.

Rice, J.R., Suo, Z., Wang, J.-S., 1990. Mechanics and thermodynamics of brittle interfacial failure in bimaterial systems. In: Rühle, M., Evans, A.G., Ashby, M.F., Hirth, J.P. (Eds.), Metal-Ceramic Interfaces. Oxford, Pergamon Press, pp. 269–294.

Ritchie, R.O., Rice, J.R., Knott, J., 1973. On the relationship between critical stress and fracture toughness in mild steel. J. Mech. Phy. Solids 21, 395–410.

Ritter, J.E., Lardner, T.J., Prakash, G.C., Stewart, A., 1994. Crack propagation in polymer adhesive-glass sandwich specimens. In: Borgesen, P., Coburn, J.C., Sanchez Jr., J.E., Rodbell, K.P. (Eds.), Materials Reliability in Microelectronics IV. Materials Research Society, pp. 599–604.

Shaw, M.C., Marshall, D.B., Dalgleish, B.J., Dadkhah, M.S., He, M.Y., Evans, A.G., 1994. Fatigue crack growth and stress redistribution at interfaces. Acta Metall. Mater. 42, 4091–4099.

Shih, C.F., 1991. Cracks on bimaterial interfaces: Elasticity and plasticity aspects. Mater. Sci. Eng. A143, 77–90.

Stern, M., 1979. Families of consistent conforming elements with singular derivative fields. Int. J. Num. Met. Eng. 14, 409–421.

Stern, M., Becker, E.B., 1978. A conforming crack tip element with quadratic variation in the singular fields. Int. J. Num. Met. Eng. 12, 279–288.

Suo, Z., Hutchinson, J.W., 1989. Sandwich test specimens for measuring interface crack toughness. Mater. Sci. Eng. A A107, 135–143.

Suo, Z., Hutchinson, J.W., 1990. Interface crack between two elastic layers. Int. J. Fract. 43, 1–18.

Varias, A.G., Suo, Z., Shih, C.F., 1991. Ductile failure of a constrained metal foil. J. Mech. Phys. Solids 39, 963–986.

Wang, H.F., Gerberich, W.W., 1993. Fracture mechanics of Ti/Al_2O_3 interfaces. Acta Metall. Mater. 41, 2425–2432.

Zienkiewicz, O.C., Taylor, R.L., 1987. The Finite Element Method. McGraw-Hill, New York, NY.